Injection mechanisms in a III -nitride light-emitting diode as seen by self-emissive electron microscopy

Tanay Tak, Cameron Johnson, Wan Ying Ho, Feng Wu, Mylène Sauty, Steve Rebollo, Andreas Schmid, Jacques Peretti, Yuh-Renn Wu, Claude Weisbuch, et al.

Identification of Injection Mechanisms in a III-Nitride Light-Emitting Diode by Self-Emissive Electron Microscopy

Tanay Tak[1,a)], Cameron W. Johnson[2], Wan Ying Ho[1], Feng Wu[1], Mylène Sauty[3], Steve Rebollo[1], Andreas K. Schmid[2], Jacques Peretti[3], Yuh-Renn Wu[4], Claude Weisbuch[1,3], and James S. Speck[1]

[1]*Materials Department, University of California, Santa Barbara, California 93106, USA*

[2]*Molecular Foundry, Lawrence Berkeley National Laboratory, Berkeley, California 94720, USA*

[3]*Laboratoire de Physique de la Matière Condensée, Ecole Polytechnique, CNRS, IP Paris, 91120 Palaiseau, France*

[4]*Graduate Institute of Photonics and Optoelectronics and Department of Electrical Engineering, National Taiwan University, Taipei 10617, Taiwan*

[a)]tak@ucsb.edu

Abstract: We report on the investigation of an electrically biased high efficiency green III-nitride light emitting diode (LED) by electron emission microscopy (EEM) using a low energy electron microscope (LEEM). The surface of the LED was activated to negative electron affinity via deposition of a sub-monolayer of Cs. With the illumination column of the LEEM turned off, upon electrical injection of the LED, we directly image the hot electrons generated by *eeh* Auger-Meitner non-radiative processes that diffuse through the top *p*-GaN layer and emit out the surface of the biased LED. By determining the source of emitted electrons using complementary electron emission spectroscopy measurements, EEM allows us to effectively map the carrier density within the LED. Using EEM, we observed non-electron emitting regions with a density of $\sim 3 \times 10^8\ cm^{-2}$, identified as V-defects. This is confirmed through the corresponding dark spots of panchromatic cathodoluminescence measurements of the same sample and by plan-view

transmission electron microscopy. The absence of electron emission at sidewall of the V-defects can be attributed to several factors including reduced carrier density in the sidewall quantum wells due to carriers traveling fast through the semipolar sidewalls before being injected into the planar quantum wells, the reduced population of hot electrons surviving diffusion through the thicker *p*-GaN filling-in the V-defect before emission onto vacuum, and a smaller Auger-Meitner coefficient for the low In content semipolar sidewall quantum wells. The stronger electron emission observed at the ridges of most V-defects compared to the planar quantum well regions indicated larger local injected carrier densities, confirming that V-defect sidewalls allow for strong lateral carrier injection when compared to the weaker vertical injection away from the V-defect as evidenced by the weaker electron emission intensity away from the V-defects.

I. Introduction

III-Nitride based light emitting diodes (LEDs) for white light illumination are one of the biggest technological achievements in energy efficiency [1,2]. However, challenges remain within III-Nitride based LEDs such as efficiency droop with increasing current density [3] and lower efficiency for longer wavelength emission [4]. Auger-Meitner [5] recombination, a three-carrier process, has been unambiguously identified as the dominant mechanism for efficiency droop via electron emission spectroscopy (EES) [6–8]. In the EES measurements, the *p*-GaN surface is the LED is activated to negative electron affinity (NEA) through the deposition of Cs [9] to allow for the emission of non-radiatively recombined hot electrons from the surface, which were then quantitatively correlated to a three-carrier process.

There is a push for long wavelength LEDs for display [10] and lighting applications [11]. Historically these LEDs have suffered reduced wall plug efficiency (WPE), compared to short wavelength III-nitride LEDs, in part due to the reduced material quality during the lower temperature quantum well (QW) growth required to incorporate higher In content [12], and larger polarization barriers to vertical carrier transport that result in excess driving voltage [13,14]. In recent years, V-defects have been proposed to reduce the forward voltage, and thus improved electrical efficiency, of long wavelength nitride-based LEDs as their semipolar sidewalls present lower polarization barriers, allowing for lateral injection of carriers into quantum wells [15–18]. V-defects are naturally occurring inverted hexagonal pyramidal structures consisting of sidewalls with six $\{1\ 0\ \bar{1}\ 1\}$ planes found in III-N crystals that form at surface perturbations, the most common of which are threading dislocations (TDs) [18]. See Fig. [injection] for a schematic showing the difference between vertical transport for injection and the proposed lateral injection

pathways using V-defect sidewalls, and the electron emission intensities expected around ideal V-defects which will be discussed more in detail later.

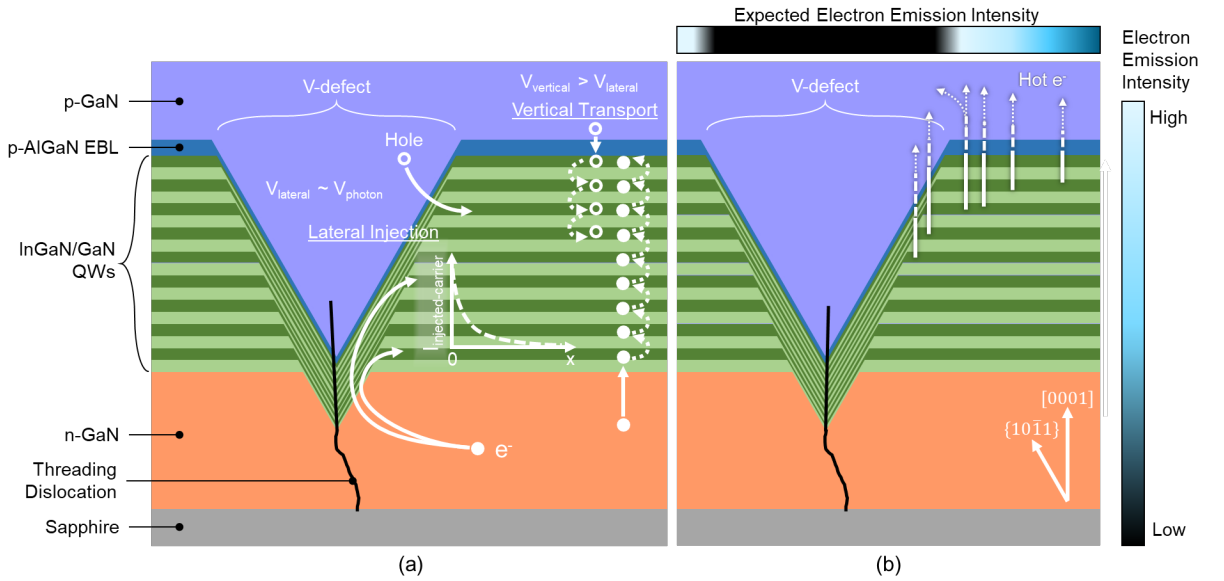

Figure [injection]. Schematic of a V-defect and planar active region of a generic LED structure showing the (a) vertical transport traditionally used to inject carriers into QWs and the proposed pathways carriers take at V-defect sidewalls to inject laterally into QWs, and (b) the pathways hot electrons take when emitting out the surface and their expected electron emission intensity. The lateral injection model is based on Ho, *et al.* [17]. V-defects are typically 100 – 300 nm wide. Note that the schematics here are not drawn to scale and merely illustrate the carrier transport mechanisms around V-defects and planar regions on an LED.

The WPE, or the ratio of light output power to electrical input power, of LEDs is given by,

$$WPE = \eta_{LEE} \times \eta_{IQE} \times \eta_{EE} \text{ and } \eta_{EE} = h\nu/eV_F \quad (1)$$

where η_{LEE} is the light extraction efficiency, describing the ratio of photons emitted from the device to the photons generated in the active region of the device, η_{IQE} is the internal quantum efficiency,

describing the ratio of the photons generated in the active region of the device to the carriers injected into the device. Lastly, η_{EE} is the electrical efficiency, where hv is the emitted photon energy, e is the fundamental charge, and V_F is the applied voltage on the device. hv/e is often referred to as the photon voltage. As seen from Eq. 1, reducing the V_F of devices can result in improvements in wall plug efficiency.

While V-defects have historically been considered deleterious to LED performance, literature dating back to 2005 invoked V-defects as a mechanism leading to suppression of nonradiative recombination by threading dislocations [19] and back to 2013 presented data showing a reduction in V_F and improved reverse voltage with intentionally formed V-defects [20], though the former authors assume that the TD propagates up through the middle of the V-defect creating a potential barrier that screens the TD, when TDs actually incline on one of the V-defect sidewalls [18], and the latter authors attribute the voltage reduction to electrical passivation of dislocations from the V-defect sidewalls. Since then, various reports on the improvement of forward voltage and thus wall-plug efficiency of LEDs with intentional V-defect nucleation have been published, experimentally demonstrating that V-defects provide beneficial carrier injection [12,21–23]. There are reports on higher-energy emission from the lower In content QWs in V-defect sidewalls measured via local excitation by scanning tunneling luminescence in a green LED [24]and observed in the electroluminescence (EL) spectra of green – red LEDs, confirmed to be coming from V-defect sidewalls via micro-photoluminescence [25], suggesting that V-defect sidewalls may have significant population of carriers from injection. Simulations also suggest that V-defects provide beneficial carrier injection [16,17], however there have not been any direct experimental demonstrations on whether carriers do in fact inject laterally.

One method to image the effects of V-defects on carrier injection is using electron emission microscopy (EEM). EEM is a newly developed technique furthering EES as it allows to map electrons emitted from a material, therefore complementing the information gained from EES on internal recombination processes with their spatial distribution [26]. Our EEM technique uses a low energy electron microscope (LEEM) [27] with its illumination column turned off, such that there is no incident electron beam on the sample and the sample itself is the electron source in this form of microscopy. The electrons emitted from the sample have been internally generated during electrical driving of the device and they escape out a surface that has been activated to NEA. EEM is thus a technique that effectively maps the carrier density in devices by imaging electrons close to the location of their generation. This self-emissive form of microscopy is like photo-electron emission microscopy (PEEM) [28] done on NEA photocathodes [29], however, EEM does not use any photon source to generate photoexcited electrons to be measured as PEEM does and instead measures the electrons generated when the sample is electrically driven. Even though EEM is a term that has been used since at least 1963 by Möllenstedt and Lenz [30] to describe electron microscopy where the imaging electrons are emitted by the sample itself, the EEM technique utilized here is different than the EEM techniques they report.

II. Challenges of Long-Wavelength GaN-Based LEDs

Phosphor converted blue GaN-based LEDs for white light illumination have had great success in replacing preceding lighting technologies as more efficient and increasingly less expensive white light sources. The peak WPE of GaN-based LEDs often exceeds 75% in the violet to blue wavelengths [31–33], however this peak efficiency decreases for longer wavelengths. There is a push to increase the efficiencies of longer wavelength GaN-based LEDs to circumvent

Stokes' losses associated with phosphor conversion for white light illumination [11] and for the development of next generation LED displays [10].

As seen in Eq. 1, there are various components that affect the efficiency of LEDs. The light extraction efficiency (LEE) has been extensively studied and modeled using ray tracing methods, where Lalau Keraly, *et al*. simulated LEDs, with conservative designs and parameters, to demonstrate LEE > 80% [34]. Better LED designs are simulated to have LEE > 90% [31,35] based on ray tracing models, and it is commonly believed that commercial LEDs are also designed with LEE ~90%. LEE values of LEDs will remain mostly unchanged for LEDs of various wavelengths, with some dependence of LEE on wavelength due to changes in refractive index.

The internal quantum efficiency (IQE) of LEDs is commonly described by the ABC model,

$$IQE = \frac{Bn^2}{An + Bn^2 + Cn^3} \tag{2}$$

where n described the carrier density in the active region, and A, B, and C are the coefficients for Shockley-Read-Hall, radiative, and Auger-Meitner recombination respectively. There is sometimes a $B'n^2$ term also added to the denominator of Eq. 2, which represents trap-assisted Auger-Meitner processes [36,37]. The IQE of III-N LEDs decreases with increasing emission wavelength beyond blue wavelengths. To realize longer wavelengths, more In content is needed in the QWs of the LED, and In incorporation increases with decreased growth temperatures which likely results in a higher density of impurities and native defects – both may behave as SRH or trap-assisted Auger-Meitner nonradiative recombination centers. There is also a larger lattice mismatch between GaN/InGaN for higher In content QWs also increases the internal electric fields in the QWs due to the discontinuity of the total polarization (spontaneous and piezoelectric) between the InGaN QW and the GaN barrier. All these effects come into play and lead to a reduction in the IQE of LEDs as they go to longer wavelengths. Differential carrier lifetime

measurements done on carefully designed and grown violet, blue, and green LEDs with a 3 nm thick single QW showed minimal change in the *A* coefficient and decreasing *B* and *C* coefficients with increasing In content, with the *C* coefficient decreasing less than the *B* coefficient with increasing In content, suggesting that decreasing radiative recombination is the leading cause of the reduction in IQE of LEDs with increasing emission wavelengths [38].

The electrical efficiency (EE) of III-N LEDs also decreases with increasing emission wavelengths. The higher In contents required for longer wavelength QWs lead to larger polarization barriers to vertical carrier transport that result in excess driving voltages for operation [13,14]. The polarization barriers and band offsets for blue LEDs are small enough such that the vertical injection of carriers can be realized at driving voltages close to the photon voltage. However, the polarization barriers and band offsets increase for longer wavelength LEDs such that large driving voltages are required for vertical transport. These large driving voltages could result in large junction biases, where a significant proportion of the injected electrons could overflow the QWs directly to the *p*-side of the diode [13,39].

Both the reduction in IQE and EE contribute to the reduced efficiencies of long-wavelength LEDs. Growth optimizations for improved material quality and cleverly designed active regions would be required to help improve IQE. Novel injection mechanisms are required to circumvent the larger barriers to vertical transport. One such method to bypass vertical transport is by using V-defect sidewalls to laterally inject carriers directly into the active region, as shown in Fig. [injection].

The National Institute of LED on Silicon Substrate team at Nanchang University, with a lot of prior simulation and experimental work done to study the effects of V-defects [40–44], published papers in 2019 [23] and 2020 [22] demonstrating world record WPEs for III-N LEDs in

the green to red wavelengths, validating the possibility of using V-defect engineering for highly efficient long wavelength LEDs. Their LEDs demonstrated operating voltages close to the photon voltage, suggesting that lateral injection through V-defects was taking place. If V-defect sidewalls allow for lateral injection, as shown in Fig. [injection], all the current flowing through the LED will preferentially inject through the V-defect and negligible vertical transport of carriers will take place. It is important to note that the peak WPEs of the long-wavelength LEDs from Nanchang University occurred at low current densities, displaying efficiency droop with increasing currents. We observe that injected carriers are insufficiently propagating away from the V-defect sidewall, leading to strong local carrier concentrations resulting in Auger-Meitner recombination, the cause of efficiency droop [6–8]

III. Electron Emission-Spectroscopy and -Microscopy of GaN-Based Devices

Electron emission spectroscopy (EES) is a technique that performs electron spectroscopy on internally generated electrons emitted from electrically biased devices. Like near-band-gap photoemission spectroscopy [45–47], this technique relies on lowering the surface vacuum energy of a *p*-type semiconductor to below the bulk conduction band minima by the deposition of Cs or Cs/O complexes to realize negative electron affinity, allowing all electrons with energies above the bulk conduction band minimum to be ejected into vacuum, the same principle by which many semiconductor photocathodes operate [48]. However, near-band-gap photoemission spectroscopy performs spectroscopy on the photoexcited electrons being emitted, while EES performs spectroscopy on the internally generated electrons emitted during electrical biasing of a device.

A significant amount of work has been performed on wurtzite GaN using both these techniques. Both near-band-gap photoemission spectroscopy and EES have been used to measure the first satellite valley energy in the conduction band of wurtzite GaN [8,47], as verified by

differential pump-probe intravalley absorption in optical experiments performed on bulk material [49], and EES has been used to measure the electron emission and hot carrier generation processes of III-N LEDs [6–8,36,50–52] and GaN *p-i-n* diodes [51,53]. The EES technique has been used to directly identify Auger-Meitner recombination as the cause of efficiency droop with increasing current for III-N LEDs [6–8], identify Trap-Assisted Auger-Meitner processes in MBE-grown III-N LEDs [36], detect a new high-energy upper valley in the conduction band of wurtzite GaN [52], and measure the minority carrier diffusion length of *p*-GaN [53,54].

As a GaN-based *p-i-n* diode or LED is turned on, electrons injected from the external circuit into the *n*-GaN will flow towards the *p*-region, undergoing drift-diffusion transport and recombination in the process. Similarly, holes injected will move towards the *n*-region. In a *p-i-n* diode, the thermalized (or overflow) electrons that cross the diode junction and survive to the vacuum exposed *p*-GaN will be emitted provided that the surface is activated to NEA, as shown schematically in Fig. [electron emission] a). For LEDs, both electrons and holes flow towards the active region of an LED, where an electron can experience five different processes: they can inject into the QWs and (i) radiatively recombine with a hole; (ii) recombine non-radiatively through a SRH process, (iii) experience band-to-band Auger-Meitner recombination; (iv) experience trap-assisted Auger-Meitner recombination; or (v) overflow the QWs directly to the *p*-region, as shown in Fig. [electron emission] b). In an LED, electrons that are generated within the active will emit out the vacuum exposed *p*-GaN provided that they survive diffusion through the top *p*-GaN (and the surface is activated to NEA). These emitted electrons may include overflow electrons, hot electrons from *eeh* Auger-Meitner processes, hot electrons from *ee* trap-assisted Auger-Meitner processes, and thermalized electrons in the top *p*-layer (band-bending region, or BBR) from energy relaxed hot electrons [7] and photogenerated electrons from Franz-Keldysh absorption. The

electron concentration in the conduction band minima of the *p*-region of a *p*-*i*-*n* diode reduces away from the junction according to

$$n_p'(x) = n_p'(0)e^{-x/L_e} \text{ and } L_e = \sqrt{D_e\tau_e} \tag{3}$$

where $n_p'(x)$ describes the number of electrons in the *p*-region with $x = 0$ as the location of the diode junction, L_e is the minority electron diffusion length, determined by D_e, the diffusion coefficient of the minority electrons, and τ_e, the average lifetime of the minority electrons. In the case of an LED, overflow carriers will follow a similar equation. However, electrons in the higher energy satellite valley diffusing from the active layer and relaxing into the Γ-valley will not follow Eq. 3, with a more complicated history of transport in both valleys and energy relaxation down from the upper valley and in the Γ-valley as hot electrons.

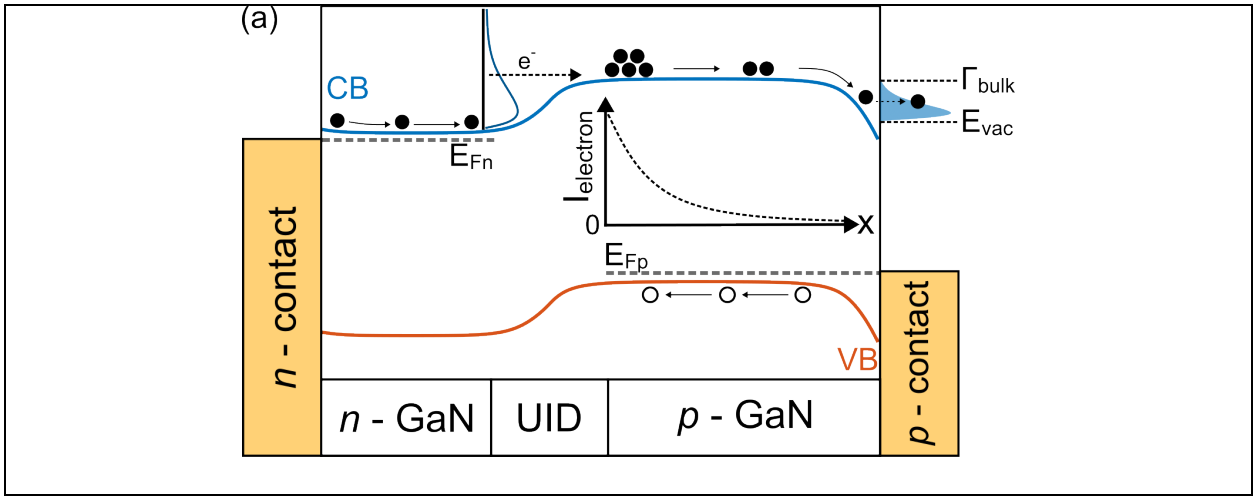

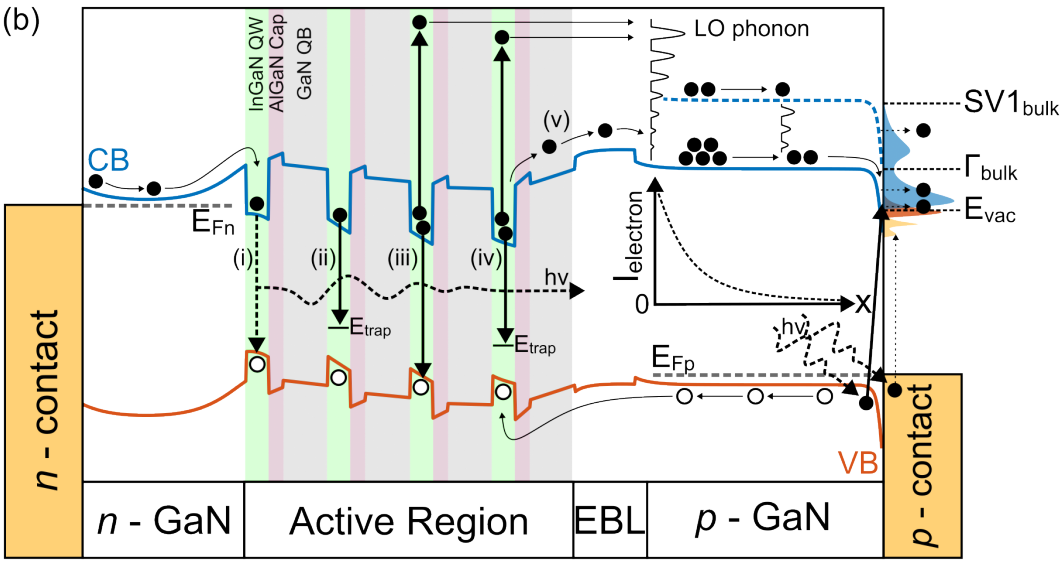

Figure [electron emission]. Schematic showing the relevant electron energy levels, transport, recombination mechanisms, and corresponding electron energy distribution curves of emitted electrons in a forward biased (a) *p-i-n* diode and (b) LED, whose surface has been activated to NEA. The electron concentration reduces further away from the junction in the *p*-GaN. The five processes electrons may experience in an LED are: (i) radiative recombination with a hole; (ii) SRH non-radiative recombination; (iii) band-to-band Auger-Meitner recombination; (iv) trap-assisted Auger-Meitner recombination; or (v) overflow to *p*-side of the LED. Note that in LEDs, it is possible to have electron emission from photoexcited electrons generated in the top *p*-layer's band-bending region and the *p*-contact by the LED light.

As mentioned earlier, EEM uses a LEEM system with its illumination column turned off to measure the electrons being emitted from the surface of a sample activated to NEA under electrical bias. A PEEM system with a modified stage allowing for electrical biasing could also be used for the EEM technique, as it requires no incident electron beam on the sample.

While there exists a report of operation of an electrically biased *p*-*n* diode in a PEEM system, the authors did not activate their sample to NEA to measure the electron emission from the electric biasing and instead measure the work function variation of the diode surface during forward, zero, and reverse bias conditions [55]. The first report of EEM from an electrically biased device whose surface has been activated to NEA has been reported by Ho, *et al*. [26]. The authors electrically bias GaN-based *p*-*i*-*n* diodes to image the thermalized electrons emitted, see Fig. [electron emission] a), and measure the lateral distribution of the junction current of the diode. We employ the same technique to image the electron emission from a biased LED, however at a much higher scale, see Fig. [electron emission] b).

IV. Experimental Methods

A commercial green ($\lambda \approx 530$ nm) LED wafer from Seoul VioSys was processed into diodes like other EES previously devices reported by our group [50]. The *p*-contact was formed using Pd/Au (50/100 nm) with a honeycomb pattern of ~5853 open 4 μm diameter circular apertures on the sample for EEM imaging, and ~4602 open hexagonal apertures with an apothem of 3.5 μm in a honeycomb pattern on the sample for EES measurements. The 4 μm diameter circular apertures and 3.5 μm apothem hexagonal apertures were chosen as bare *p*-GaN was simulated to spread current uniformly without the use of a current spreading layer at low current densities for these dimensions [56]. A C-shaped *n*-contact partially surrounding the *p*-contact and *p*-pad was formed by reactive ion etching using BCl_3/Cl_2 for the EEM sample and $SiCl_4$ for the EES sample into the *n*-region and contacted by Ti/Au (30/300 nm). Note that the difference in etch chemistries was due to supply chain constraints during the different processing runs for the EES and the EEM samples.

An ultrahigh-vacuum (UHV) EES system at UCSB, as described elsewhere [7], was used to measure the energy distribution curves of the emitted electrons from the electrically biased LED. The sample was cleaned and introduced into the UHV EES system, where a submonolayer of Cs was deposited onto the surface using a SAES Getters cesium source. By monitoring photoexcited electrons emitted from *p*-GaN during Cs deposition, we confirmed that NEA was achieved. EES was performed with the device under cw operation for varying injection currents. The energy of the emitted electrons was measured referenced to the Fermi level of the *p*-contact using a Comstock AC-901 spherical sector electrostatic analyzer operated in constant pass energy mode with an energy resolution of 90 meV.

The ELMITEC LEEM III system at the Molecular Foundry of the Lawrence Berkeley National Lab with a spin polarized electron gun source [57] was used as the LEEM instrument. A layout of the electron optics of the LEEM system operating in EEM mode is shown in Fig. [optics], where the imaging detector is a fiber-coupled scintillator-based CMOS camera (TVIPS TemCam-F216 [58]). The camera is reported to have a non-linearity factor of <1%, suggesting that the intensity of electrons measured while imaging scales linearly with the number of electrons detected. The sample stage was modified to allow for electrical driving of devices *in vacuo* with an external voltage source, as shown in Fig. [sample stage].

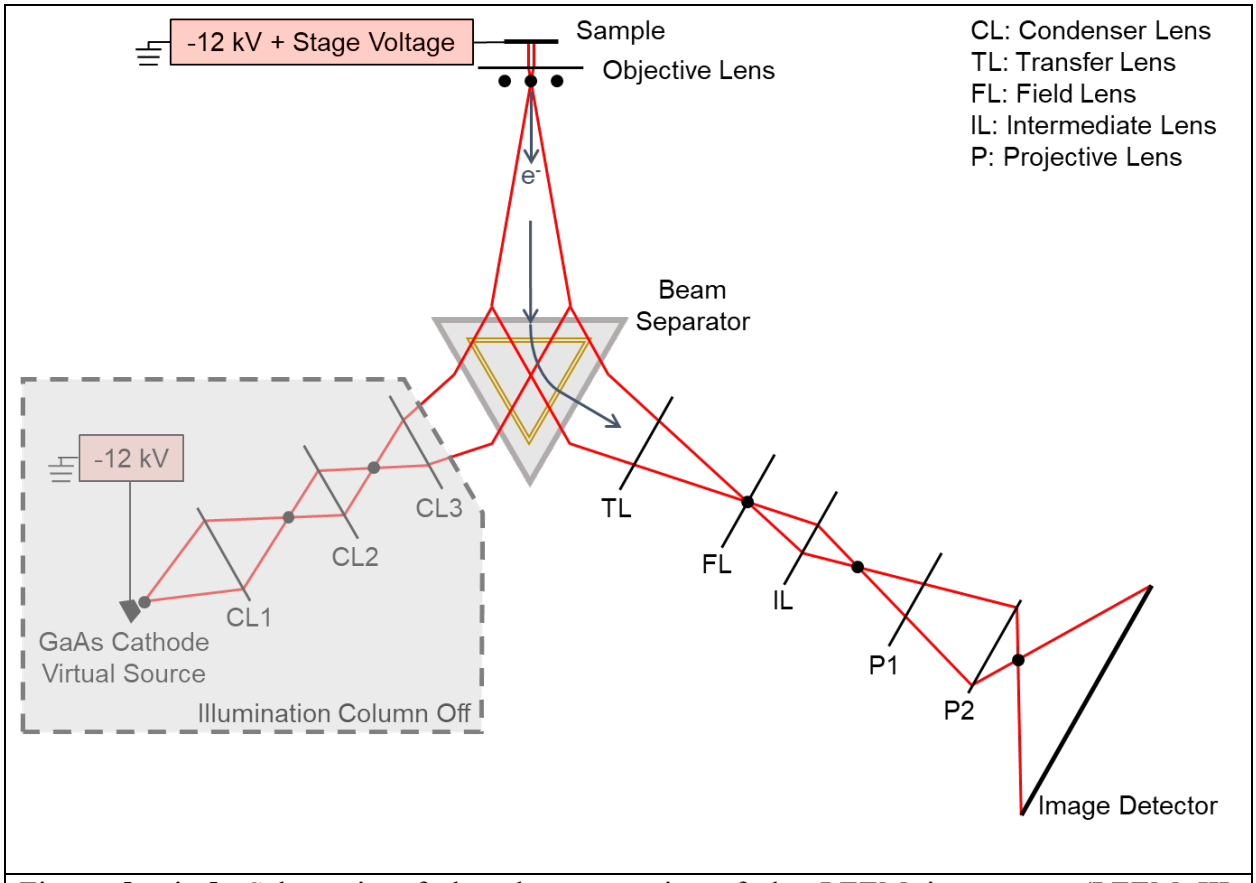

Figure [optics]. Schematic of the electron optics of the LEEM instrument (LEEM III, ELMITEC) as used during EEM mode. The e-gun (GaAs Cathode) and sample are at high voltage while all the magnetic lenses are grounded.

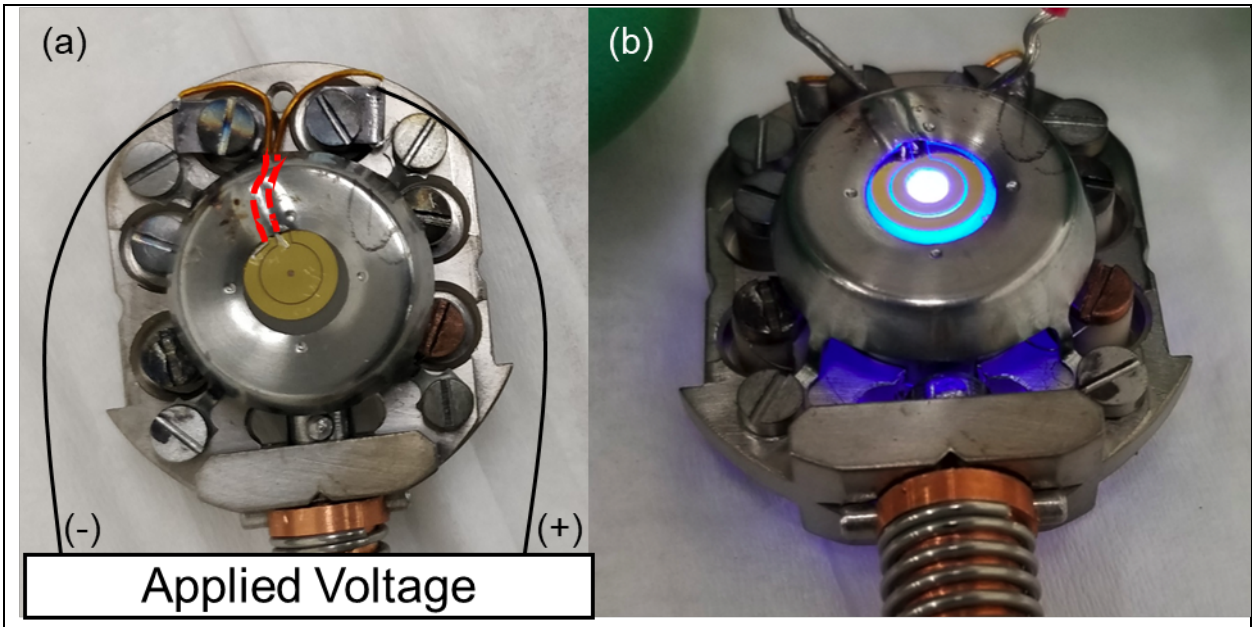

Figure [sample stage]. The modified sample stage used to allow for electrical driving of devices, where (a) shows the wiring connections to the sample stage, with the dashed red lines indicating the route the Teflon coated wires take under the sample cover and (b) shows an externally electrically driven blue LED on the sample stage.

The sample was cleaned using a HCl:isopropanol solution to remove any surface oxides and dried with N_2 prior to introduction into the LEEM system [59,60]. This surface treatment has been found to remove surface oxygen effectively tying up the dangling bonds with Cl instead and hindering reoxidation, as verified by Auger-Meitner electron spectroscopy. No flash annealing or high temperature cleaning was performed *in vacuo*, as such procedures were found to degrade the *p*-contact. Cs was deposited onto the sample using a SAES Getters Cs source to activate the sample to NEA. Work function measurement of the exposed cesiated *p*-GaN in the circular aperture of the sample confirmed that the vacuum level was below the bulk conduction band minimum [26,61]. We operated the LEEM system at a fixed magnification where the electron optics setting used

limited our resolution. With a constant distance between objective lens and the sample and using a single field of view, we determined that each pixel in EEM corresponded to ~28 nm × 28 nm, calibrated using the lithographically defined apertures on our sample.

Cathodoluminescence (CL) measurements were performed using a Gatan MonoCL4 [62] with mono- and pan-chromatic capabilities attached to a field emission scanning electron microscope (Thermo Fisher Apreo C LoVac SEM [63]) operating at 15 kV with a beam current of 1.6 nA. Transmission electron microscopy (TEM) was performed with a ThermoFisher G2 F200X TEM/STEM system [64] operated at 200 kV. The TEM sample was prepared by focused ion beam (FIB) using an FEI Helios Dualbeam Nanolab 600 instrument [65]. Secondary ion mass spectroscopy (SIMS) was performed using a Cameca IMS 7f-Auto [66]. Atomic force microscopy (AFM) was performed using an Asylum MFP-3D [67] operating in tapping mode.

V. Results and Discussion

The LED materials were characterized using SIMS, TEM, and AFM, as shown in Fig. [SG1905]. SIMS was used to determine the epitaxial structure of the LED, as shown in Fig. [SG1905] a), which helped educate the etch depth required while processing devices. 20 × 20 μm^2, 5 × 5 μm^2, and 2 × 2 μm^2 scans were performed with the AFM, giving a root mean square (RMS) roughness of 1.64 nm, 0.462 nm, and 0.331 nm, respectively. These low RMS values, alongside the steps visible in Fig. [SG1905] c) from the step-flow growth of GaN, and the *p*-GaN filling in the V-defect visible in Fig. [SG1905] b), demonstrate that the *p*-GaN surface is planar. Planar surfaces are of importance to EEM measurements as varying surface potentials from topography variations would affect electron emission properties, however that is not an issue in this wafer.

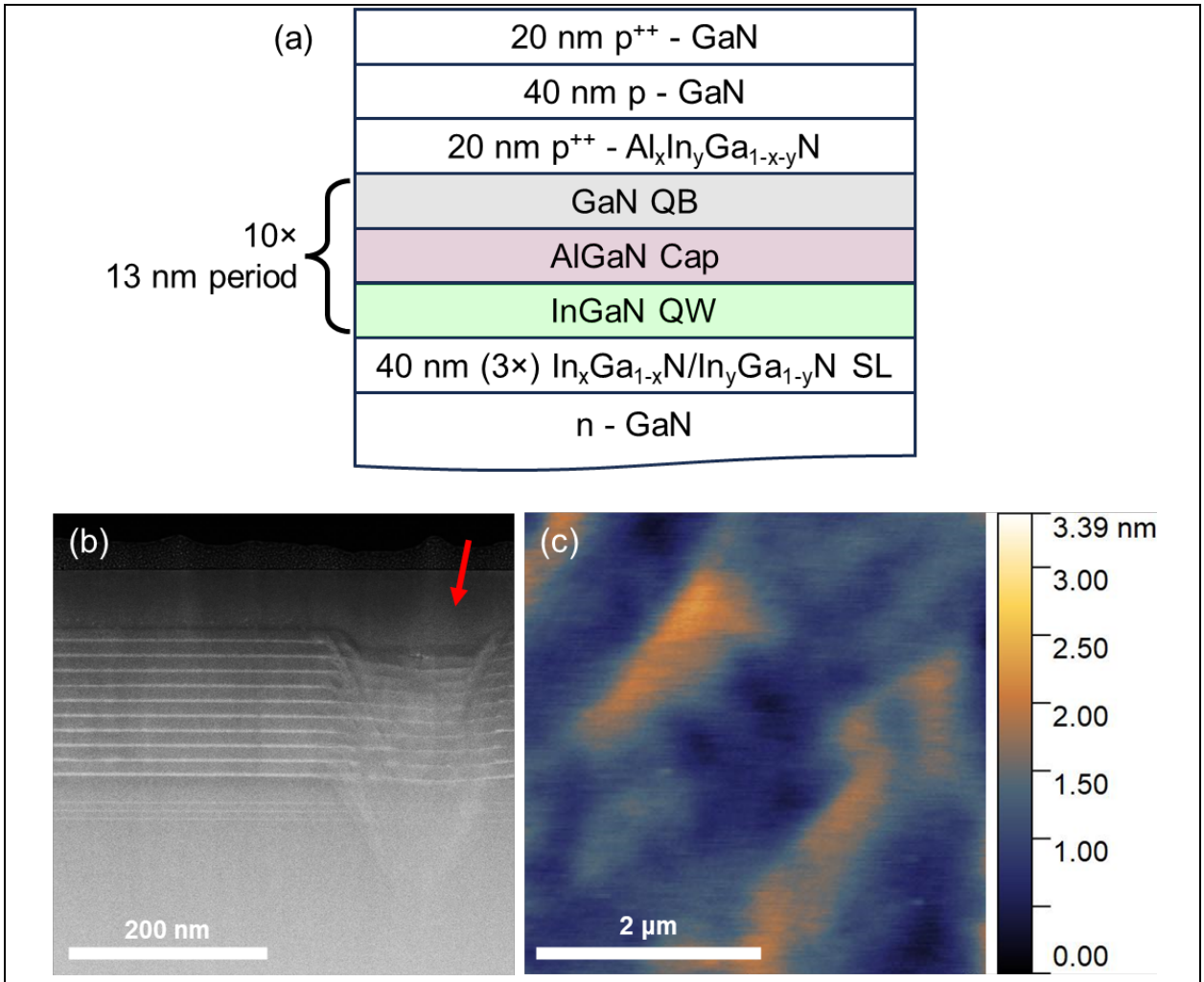

Figure [SG1905]. (a) Epitaxial structure of the LED, as determined using SIMS. (b) High-angle angular dark field STEM image of a cross-section of the LED, with a visible V-defect as indicated by the red arrow. (c) AFM scan of the sample surface.

Once the devices were fabricated, their current-voltage's (I-V) were measured, as shown in Fig. [IV] a) and b). The optical emission wavelength of the EES device was also measured with a spectrometer, and peak wavelengths for various currents plotted in Fig. [IV} c). The EEM device had an increased leakage current, as seen in Fig. [IV] b), which can be attributed to the GaN pillars left in the etched trenches during the BCl_3/Cl_2 etch of the *n*-side [68]. The I-V curve of the EEM

sample after an arcing event, which will be described later, is also presented. The blue-shift in the EL emission spectra observed with increasing current, is commonly observed in GaN-based LEDs and is attributed to the charge screening of the polarization related electric field with increased carriers due to the quantum confined stark effect.

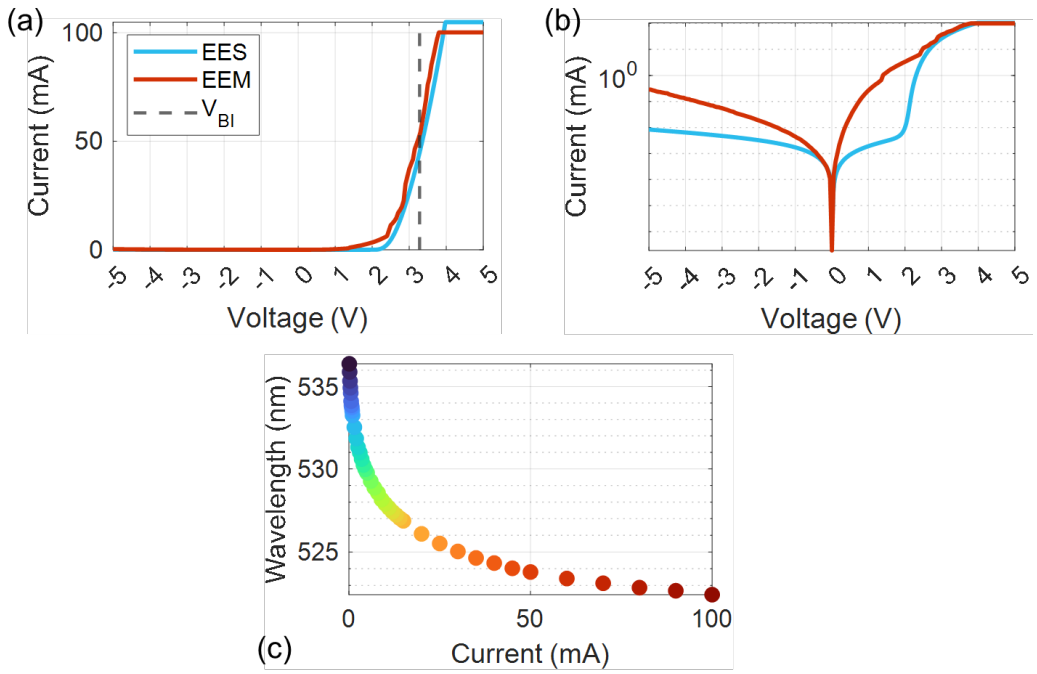

Figure [IV]. I-V curves for the EES and EEM device shown in (a) linear and (b) semilogarithmic scale. (c) Peak wavelength from EL for the EES sample at varying bias currents. Note that the dashed line in (a) indicates the V_{BI} of the LED calculated based on doping concentrations measured via SIMS; both devices have a junction bias below V_{BI} for operation under ~50 mA.

As mentioned earlier, in an LED, electrons that are generated within the active region that survive diffusion through the top *p*-GaN and emit out the vacuum exposed *p*-GaN will be emitted provided that the surface is activated to NEA. The energy distribution curves (EDCs) of these emitted electrons were measured using EES and are shown in Fig. [EES] for varying bias currents. The EDCs show five distinct peaks: (i) Au; and (ii) Pd photoemission peak from the electrons

photoexcited from the device *p*-contact; (iii) BBR peak corresponding to thermalized electrons generated in the BBR from energy relaxed hot electrons or sub-bandgap photoemission through Franz-Keldysh absorption [7]; (iv) emission from the Γ-valley of the bulk GaN; and (v) emission from a higher energy side-valley of the bulk GaN. Peaks with a semiconductor origin are expected to have energies that increase with the applied bias due to the voltage drop from the *p*-contact to the sample surface [7,50,51], which validates our peak assignments shown in Fig. [EES] a) as the BBR, Γ valley, and satellite valley (SV) peaks, which have semiconductor origins, move to higher energies with increased diode bias. Further, we fitted the peaks to exponentially modified gaussian functions [54] to find their integrated intensities. These integrated intensities were analyzed as done in Ho, *et al*. [6], and yielded the same result that the emitted electrons populating the SV peak are correlated to a three-body process (Auger-Meitner recombination).

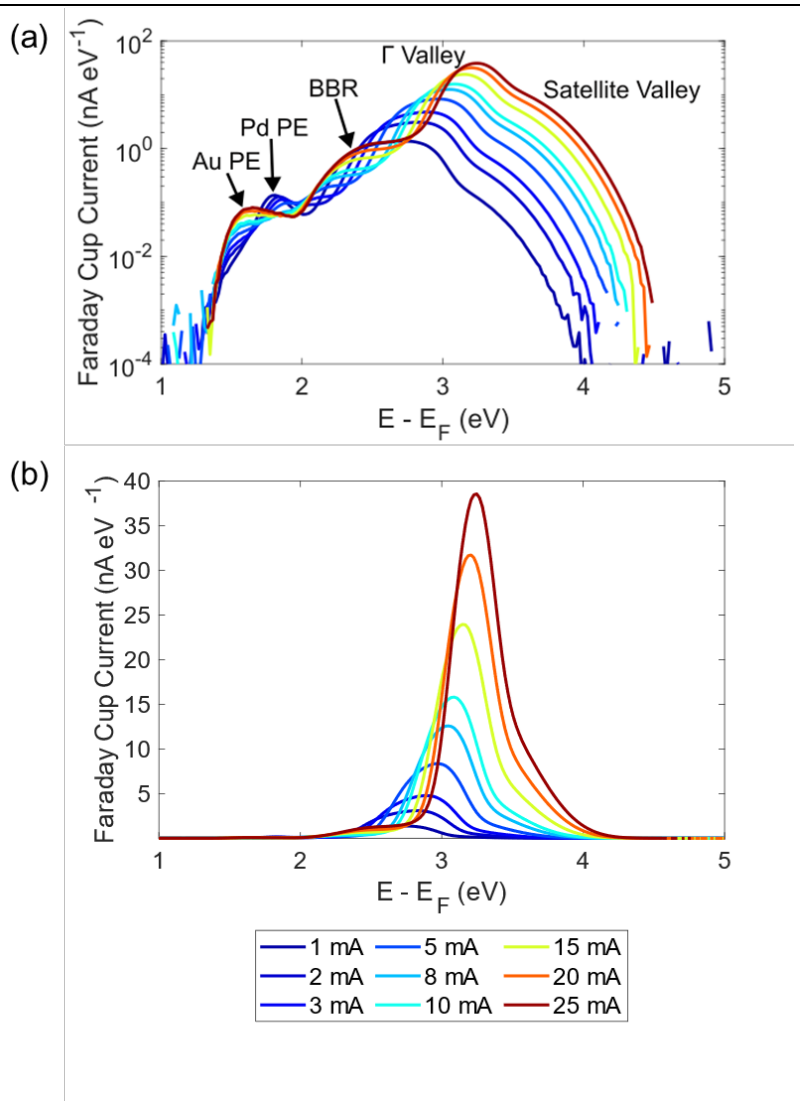

Figure [EES]. EDCs of the green LED EES device plotted in (a) semilogarithmic and (b) linear scale for varying bias currents. (a) Labels the origins of the various electron emission peaks based on Ho, *et al*. [6].

The built-in voltage of the LED is calculated using

$$V_{BI} \approx \frac{E_G}{e} + \frac{k_B T}{e} ln\left(\frac{N_D N_A}{N_C N_V}\right) \tag{4}$$

where E_G is the bandgap of GaN, N_D and N_A are the donor and acceptor concentration in *n*- and *p*-GaN, respectively, and N_C and N_V are the effective density of states in the conduction and valence bands, respectively. For the measured doping via SIMS, we calculate V_{BI} to be 3.28 V. As our devices are measured with operating voltages below $V_{BI,}$ as shown in Fig. [IV] a), we expect the junction bias to be below V_{BI} and there to be no overflow electrons contributing to the Γ-valley [39]. EDC data shows increasing electron emission from the Γ-valley and higher energy side-valley with increasing bias, originating from increased *eeh* Auger-Meitner processes [6]. Fig. [EES] shows that for moderate to large bias currents, the largest contributor to electron emission was from *eeh* Auger-Meitner processes, which populate the Γ-valley and the side-valley peaks, and thus *eeh* Auger-Meitner processes would dominate the electron emission imaged via EEM. As electron emitting Auger-Meitner is a three-carrier process, greater electron emission would be expected in regions with increased carrier density present and EEM would map the cube of the carrier density (n^3) in the device.

EEM images of the green LED show non-electron emitting regions, the dark spots as seen in Fig. [EEM] a), with densities of $\sim 3 \times 10^8\ cm^{-2}$, that we suspected were V-defects. Dark spots in panchromatic CL measurements, Fig. [microscopy] a), on the same sample indicated a threading dislocation density of $\sim 3 \times 10^8\ cm^{-2}$ as well and visually shared a similar distribution as the EEM dark spots, further agreeing with our initial assignment of the dark regions in the EEM images to V-defects. CL measurements on the same location as the EEM measurements were not pursued as finding the same few apertures to measure in a pool of over 5800 apertures, along with an imperfect metal lift-off, as shown in Fig. [microscopy] c), during the device processing would be challenging. Furthermore, we noticed while testing various devices that the device would have minimal illumination, if any, if the device had undergone an arcing event in the LEEM system,

yielding low counts in CL measurements. Arcing events most occurred when raising the sample to the high stage voltage after Cs deposition, possibly due to the additional photogenerated electrons being emitted from the NEA surface. These arcing events increased device leakage sometimes entirely suppressing the LEDs luminescence making them useless for CL measurements. We believe an improved stage design, operating the LEEM at even lower voltages, and modifying the device mask are some ways we can prevent arcing events in the future.

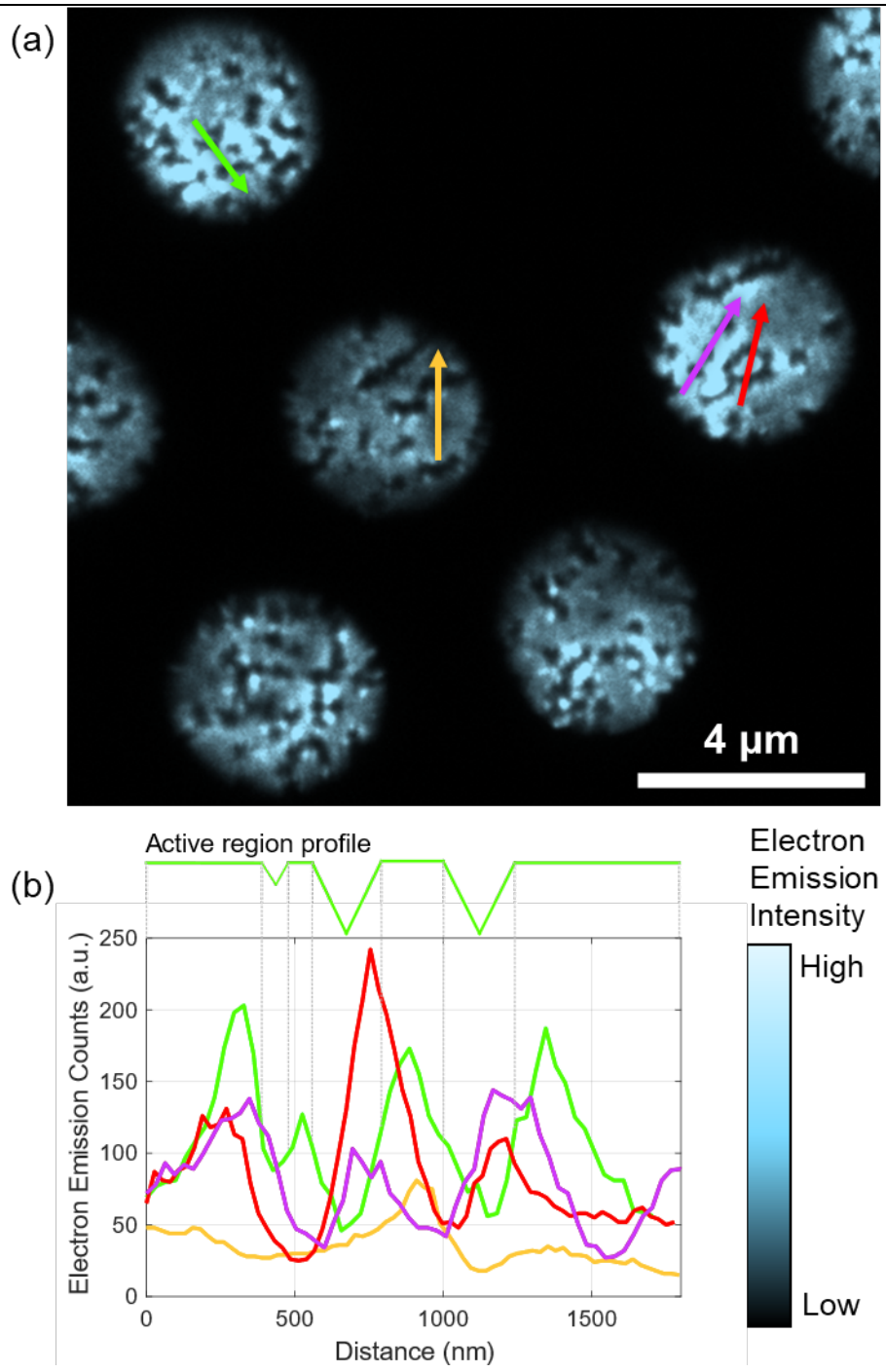

Figure [EEM]. (a) Electron emission microscopy of the green LED EEM device operating at 8 mA. (b) Electron emission count profiles along the lines labeled in (a). The electron emission counts are linearly proportional to the number of electrons being emitted.

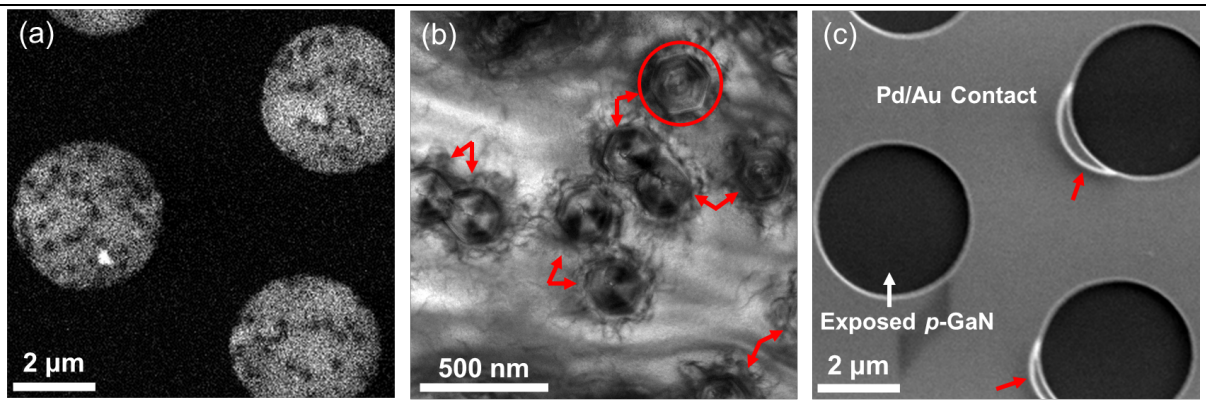

Figure [microscopy]. (a) panchromatic CL of the same sample at different apertures, (b) zone-axis plan-view TEM of a different sample from the same LED wafer, and (c) SE-SEM micrographs corresponding to the CL measurements of the green LED. The red circle in (b) indicates a single hexagonal V-defect with red arrows indicating the others. The red arrows in (c) point to regions with imperfect metal lift-off during processing. (b) has been modified from [69]

Plan-view TEM of a different sample from the same wafer showed hexagonal features, corresponding to V-defects, as seen in Fig. [microscopy] b), with a density of $\sim 3 \times 10^8\ cm^{-2}$. The size and distribution of these V-defects was also identical to the EEM dark spot dimensions, confirming that the EEM dark spots were V-defects. Note that there would be a lateral spread of the *eeh* Auger-Meitner generated electrons as they are diffusing through the *p*-GaN of a similar length scale as the diffusion length of *p*-GaN, which would change the shape of the non-electron emitting regions from the expected hexagonal one, which may explain why they appear mostly circular in Fig. [EEM] a). The thickness of the *p*-region of the LED varies based on its location on planar QW regions or above V-defects, as seen in Fig. [SG1905]. The *p*-region thickness in this LED is ~70 nm above planar QWs but can get up to ~300 nm for filled in V-defects that have nucleated prior to the active region based on cross-section TEM. These thicknesses were

confirmed by measuring a depth profile of the concentration of Mg, the commonly used *p*-type dopant for GaN, by SIMS. High concentrations were observed in the top 80 nm after which a sharp drop occurs, followed by a slow decay in concentration corresponding to the *p*-GaN filled in the V-defects, before reaching the SIMS noise level at 300 nm. The minority carrier diffusion length in *p*-GaN has been measured to be ~10 and ~26 nm by EES for doping concentrations of 2×10^{20} cm^{-3} and 3.5×10^{19} cm^{-3}, respectively [53,54], which are close to the ~28 nm/pixel resolution of the EEM measurement.

There may be various reasons why V-defects are non-electron emitting regions, such as fewer minority carriers, hot or thermalized, survive diffusing through the thicker *p*-GaN capping the V-defect before escaping, low carrier density in the sidewall QWs due to their fast traveling to inject laterally and efficiently into planar quantum wells as simulations predict, and a reduced hot carrier emission stemming from the lower Auger-Meitner coefficient for the semipolar sidewalls [70,71]. Electron emission counts are highest adjacent to V-defects, the lower electron emission count regions, as seen in Fig. [EEM] b). Stronger electron emission is also observed at the ridges of most V-defects, as seen in Fig. [EEM] a), providing evidence that carriers are injected laterally and efficiently into planar quantum wells. Lateral injection of carriers through V-defect sidewalls implies larger injected carrier densities present immediately outside the V-defect sidewalls which would cause an increased amount of Auger-Meitner recombination and thus lead to stronger electron emission, exactly as we observe. Further away from the edge of the defect, carriers diffuse and recombine, hence the lower hot carrier generation as evidenced by the fainter electron emission. These lateral injection results agree with simulations that electron travel up the sidewalls of V-defects that have been nucleated prior to the active region growth and directly inject themselves into the quantum wells in the active region [17].

Fig. [injection] b) presents a model of the pathways carriers take around ideal V-defects, based on [18], and shows the expected electron emission intensity around the V-defect region, which agrees well with our observation as shown in Fig. [EEM] a). Simulations from Ho, *et al*. [17], also show that with an increased V-defect density, larger planar regions of the top QWs have radiative recombination, indicating extended significant carrier concentration. We also observe increased electron emission in regions with increased V-defect density, suggesting that the top QWs are more uniformly populated with injected carriers, which are generating and emitting *eeh* Auger-Meitner electrons. This confirmation of the injection mechanism from V-defect sidewalls directly shows their benefits. However, further studies must be performed to identify the effects that V-defects that do not nucleate prior to the active region have on the carrier injection as they have been attributed to non-radiative centers [12]. These "bad" V-defects nucleate in the active region of the LED and are associated with stacking fault boxes [18]. It is also noticed in Fig. [EEM] a) that not all sides of the V-defects have stronger electron emission, suggesting that lateral carrier injection may not take place through all the sidewalls of the V-defects. This agrees with the recent finding that threading dislocations incline on the face of one of the six sidewalls of the V-defects [18] and may act as a non-radiative recombination center.

As the imaging detector on the LEEM system can linearly measure electron counts, we can measure the reduction of electron emission intensities from V-defect edges to planar regions to estimate the lateral diffusion length of injected carriers in the InGaN QWs. Since electrons generated from *eeh* Auger-Meitner processes can only be excited to higher energies with the energy transfer from an *e-h* recombination, their observation near the V-defect position shows that we are injecting both carriers from the V-defect and we assume here that both the laterally injected electrons and holes follow ambipolar diffusion and participate in the hot electron generation

process. We can then estimate the current of injected carriers x distance away from the V-defect sidewall using

$$I_{injected}(x) \propto I_a P_{esc} e^{-x/L_a} \quad (5)$$

where I_a is the injected current at the V-defect sidewall, P_{esc} is the escape probability of the electrons emitting the surface and is assumed to be uniform across the sample due to uniform deposition of cesium [26,61], and L_a is the lateral ambipolar carrier diffusion length of injected carriers.

Determining the distance that the electron emission intensity drops by $e^{-1} \approx 0.37$ from the peak electron emission intensity at the edge of V-defects gives us a good estimate of the lateral diffusion length of injected carriers. We estimate L_a to be ~ 30 – 300 nm across various V-defects, which matches well with the ~ 320 nm ambipolar diffusion length measured for $In_{0.08}Ga_{0.92}N$ [72] and the ~ 345 – 370 nm ambipolar diffusion length measured for $In_{0.13}Ga_{0.87}N$ [73], where the higher In content of the green QWs in the measured EEM sample may explain the lower values. We speculate that by increasing the resolution of the EEM system and measuring the intensities of injected carriers on well-behaved V-defects, we can further study the carrier transport of these injected carriers. Gaining a better understanding of the carrier transport of laterally-injected carriers can help inform simulations of LEDs to help optimize V-defect size, density, and distribution to create more efficient long wavelength nitride-based LEDs.

Apart from predicting the lateral injection at V-defect sidewalls, the simulations reported in [18] also show a more uniform injection into deeper QWs as a consequence of the lateral injection that V-defects provide. Uniform injection into QWs provides an opportunity to mitigate efficiency droop at high current densities as there would be less accumulation of carriers only in

the top QWs and reduced Auger-Meitner recombination. Further work must be performed to validate whether these beneficial V-defects allow for depth-uniform injection of QWs.

VI. Conclusion

In summary, we describe here the use of EEM [26] to effectively map the carrier density in an electrically driven III-nitride LED. Non-electron emitting regions were observed and attributed to V-defects, as verified by panchromatic CL and plan-view TEM measurements, allowing us to directly image the internal microstructure using this self-emission technique. We observe increased electron emission at the ridges of V-defects that we attribute to lateral carrier injection through the sidewalls of V-defects. Direct imaging of the electrons generated from *eeh* Auger-Meitner processes, as verified by complementary EES measurements, emitted from the LED surface confirms the proposed current pathway of lateral injection through V-defect sidewalls.

Acknowledgements

Support at UCSB was provided by the Solid State Lighting and Energy Electronics Center (SSLEEC); U.S. Department of Energy under the Office of Energy Efficiency & Renewable Energy (EERE) Award No. DE-EE0009691; the University of California, Santa Barbara (UCSB) – Collaborative Research of Engineering, Science and Technology (CREST) program; the National Science Foundation (NSF) RAISE program (Grant No. DMS-1839077); the Simons Foundation (Grant #s 601952 and 1027114 for JSS and CW, respectively). A portion of this work was performed in the UCSB Nanofabrication Facility, an open access laboratory. The MRL Shared Experimental Facilities are supported by the MRSEC Program of the NSF under Award No. DMR

1720256. Work at the Molecular Foundry was supported by the Office of Science, Office of Basic Energy Sciences, of the U.S. Department of Energy under Contract No. DE-AC02-05CH11231.

References

[1] S. P. Denbaars, D. Feezell, K. Kelchner, S. Pimputkar, C.-C. Pan, C.-C. Yen, S. Tanaka, Y. Zhao, N. Pfaff, R. Farrell, M. Iza, S. Keller, U. Mishra, J. S. Speck, and S. Nakamura, *Development of Gallium-Nitride-Based Light-Emitting Diodes (LEDs) and Laser Diodes for Energy-Efficient Lighting and Displays*, Acta Mater **61**, 945 (2013).

[2] J. Heber, *Nobel Prize 2014: Akasaki, Amano & Nakamura*, Nat Phys **10**, 791 (2014).

[3] J. Cho, E. F. Schubert, and J. K. Kim, *Efficiency Droop in Light-Emitting Diodes: Challenges and Counter Measures*, Laser Photon Rev **7**, 408 (2013).

[4] M. Auf Der Maur, A. Pecchia, G. Penazzi, W. Rodrigues, and A. Di Carlo, *Efficiency Drop in Green InGaN/GaN Light Emitting Diodes: The Role of Random Alloy Fluctuations*, Phys Rev Lett **116**, 027401 (2016).

[5] D. Matsakis, A. Coster, B. Laster, and R. Sime, *A Renaming Proposal: "The Auger–Meitner Effect,"* Phys Today **72**, 10 (2019).

[6] W. Y. Ho, Y. C. Chow, D. J. Myers, F. Wu, J. Peretti, C. Weisbuch, and J. S. Speck, *Quantitative Correlation of Hot Electron Emission to Auger Recombination in the Active Region of C-Plane Blue III-N LEDs*, Appl Phys Lett **119**, 51105 (2021).

[7] J. Iveland, L. Martinelli, J. Peretti, J. S. Speck, and C. Weisbuch, *Direct Measurement of Auger Electrons Emitted from a Semiconductor Light-Emitting Diode under Electrical Injection: Identification of the Dominant Mechanism for Efficiency Droop*, Phys Rev Lett **110**, 177406 (2013).

[8] J. Iveland, M. Piccardo, L. Martinelli, J. Peretti, J. W. Choi, N. Young, S. Nakamura, J. S. Speck, and C. Weisbuch, *Origin of Electrons Emitted into Vacuum from InGaN Light Emitting Diodes*, Appl Phys Lett **105**, 52103 (2014).

[9] O. E. Tereshchenko, G. É. Shaĭbler, A. S. Yaroshevich, S. V. Shevelev, A. S. Terekhov, V. V. Lundin, E. E. Zavarin, and A. I. Besyul'kin, *Low-Temperature Method of Cleaning p-GaN(0001) Surfaces for Photoemitters with Effective Negative Electron Affinity*, Physics of the Solid State **46**, 1949 (2004).

[10] M. S. Wong, S. Nakamura, and S. P. DenBaars, *Review—Progress in High Performance III-Nitride Micro-Light-Emitting Diodes*, ECS Journal of Solid State Science and Technology **9**, 015012 (2020).

[11] DOE BTO Solid-State Lighting Program, 2022 DOE SSL R&D Opportunities, 2022.

[12] J. Ewing, C. Lynsky, J. Zhang, P. Shapturenka, M. Wong, J. Smith, M. Iza, J. S. Speck, and S. P. DenBaars, *Influence of Superlattice Structure on V-Defect Distribution, External Quantum Efficiency and Electroluminescence for Red InGaN Based MLEDs on Silicon*, Crystals (Basel) **12**, 1216 (2022).

[13] G. Lheureux, C. Lynsky, Y.-R. Wu, J. S. Speck, and C. Weisbuch, *A 3D Simulation Comparison of Carrier Transport in Green and Blue C-Plane Multi-Quantum Well Nitride Light Emitting Diodes*, J Appl Phys **128**, 235703 (2020).

[14] C. Lynsky, A. I. Alhassan, G. Lheureux, B. Bonef, S. P. Denbaars, S. Nakamura, Y. R. Wu, C. Weisbuch, and J. S. Speck, *Barriers to Carrier Transport in Multiple Quantum Well Nitride-Based c -Plane Green Light Emitting Diodes*, Phys Rev Mater **4**, 054604 (2020).

[15] Z. Quan, L. Wang, C. Zheng, J. Liu, and F. Jiang, *Roles of V-Shaped Pits on the Improvement of Quantum Efficiency in InGaN/GaN Multiple Quantum Well Light-Emitting Diodes*, J Appl Phys **116**, (2014).

[16] C. K. Li, C. K. Wu, C. C. Hsu, L. S. Lu, H. Li, T. C. Lu, and Y. R. Wu, *3D Numerical Modeling of the Carrier Transport and Radiative Efficiency for InGaN/GaN Light Emitting Diodes with V-Shaped Pits*, AIP Adv **6**, 55208 (2016).

[17] C. H. Ho, J. S. Speck, C. Weisbuch, and Y. R. Wu, *Efficiency and Forward Voltage of Blue and Green Lateral LEDs with V-Shaped Defects and Random Alloy Fluctuation in Quantum Wells*, Phys Rev Appl **17**, 014033 (2022).

[18] F. Wu, J. Ewing, C. Lynsky, M. Iza, S. Nakamura, S. P. Denbaars, and J. S. Speck, *Structure of V-Defects in Long Wavelength GaN-Based Light Emitting Diodes*, J Appl Phys **133**, 035703 (2023).

[19] A. Hangleiter, F. Hitzel, C. Netzel, D. Fuhrmann, U. Rossow, G. Ade, and P. Hinze, *Suppression of Nonradiative Recombination by V-Shaped Pits in GaInN/GaN Quantum Wells Produces a Large Increase in the Light Emission Efficiency*, Phys Rev Lett **95**, 127402 (2005).

[20] S. H. Han, D. Y. Lee, H. W. Shim, J. Wook Lee, D. J. Kim, S. Yoon, Y. Sun Kim, and S. T. Kim, *Improvement of Efficiency and Electrical Properties Using Intentionally Formed V-Shaped Pits in InGaN/GaN Multiple Quantum Well Light-Emitting Diodes*, Appl Phys Lett **102**, 251123 (2013).

[21] C. Lynsky, R. C. White, Y. C. Chow, W. Y. Ho, S. Nakamura, S. P. DenBaars, and J. S. Speck, *Role of V-Defect Density on the Performance of III-Nitride Green LEDs on Sapphire Substrates*, J Cryst Growth **560–561**, 126048 (2021).

[22] S. Zhang, J. Zhang, J. Gao, X. Wang, C. Zheng, M. Zhang, X. Wu, L. Xu, J. Ding, Z. Quan, and F. Jiang, *Efficient Emission of InGaN-Based Light-Emitting Diodes: Toward Orange and Red*, Photonics Res **8**, 1671 (2020).

[23] F. Jiang, J. Zhang, L. Xu, J. Ding, G. Wang, X. Wu, X. Wang, C. Mo, Z. Quan, X. Guo, C. Zheng, S. Pan, and J. Liu, *Efficient InGaN-Based Yellow-Light-Emitting Diodes*, Photonics Res **7**, 144 (2019).

[24] M. Sauty, N. Alyabyeva, C. Lynsky, Y. C. Chow, S. Nakamura, J. S. Speck, Y. Lassailly, A. C. H. Rowe, C. Weisbuch, and J. Peretti, *Probing Local Emission Properties in InGaN/GaN Quantum Wells by Scanning Tunneling Luminescence Microscopy*, Physica Status Solidi (B) **260**, 2200365 (2023).

[25] Y. C. Chow, T. Tak, F. Wu, J. Ewing, S. Nakamura, S. P. DenBaars, Y.-R. Wu, C. Weisbuch, and J. S. Speck, *Origins of the High-Energy Electroluminescence Peaks in Long-Wavelength (∼495–685 Nm) InGaN Light-Emitting Diodes*, Appl Phys Lett **123**, (2023).

[26] W. Y. Ho, C. W. Johnson, T. Tak, M. Sauty, Y. C. Chow, S. Nakamura, A. Schmid, J. Peretti, C. Weisbuch, and J. S. Speck, *Steady-State Junction Current Distribution in p-n GaN Diodes Measured Using Low-Energy Electron Microscopy (LEEM)*, Appl Phys Lett **123**, 031101 (2023).

[27] E. Bauer, *Low Energy Electron Microscopy*, Reports on Progress in Physics **57**, 895 (1994).

[28] E. Bauer, M. Mundschau, W. Swiech, and W. Telieps, *Surface Studies by Low-Energy Electron Microscopy (LEEM) and Conventional UV Photoemission Electron Microscopy (PEEM)*, Ultramicroscopy **31**, 49 (1989).

[29] X. Jin, A. A. C. Cotta, G. Chen, A. T. N'Diaye, A. K. Schmid, and N. Yamamoto, *Low Energy Electron Microscopy and Auger Electron Spectroscopy Studies of Cs-O Activation Layer on p-Type GaAs Photocathode*, J Appl Phys **116**, 34 (2014).

[30] G. Möllenstedt and F. Lenz, *Electron Emission Microscopy*, Advances in Electronics and Electron Physics **18**, 251 (1963).

[31] L. Y. Kuritzky, A. C. Espenlaub, B. P. Yonkee, C. D. Pynn, S. P. DenBaars, S. Nakamura, C. Weisbuch, and J. S. Speck, *High Wall-Plug Efficiency Blue III-Nitride LEDs Designed for Low Current Density Operation*, Opt Express **25**, 30696 (2017).

[32] Y. Narukawa, M. Ichikawa, D. Sanga, M. Sano, and T. Mukai, *White Light Emitting Diodes with Super-High Luminous Efficacy*, J Phys D Appl Phys **43**, 354002 (2010).

[33] C. A. Hurni, A. David, M. J. Cich, R. I. Aldaz, B. Ellis, K. Huang, A. Tyagi, R. A. DeLille, M. D. Craven, F. M. Steranka, and M. R. Krames, *Bulk GaN Flip-Chip Violet Light-Emitting Diodes with Optimized Efficiency for High-Power Operation*, Appl Phys Lett **106**, 031101 (2015).

[34] C. Lalau Keraly, L. Kuritzky, M. Cochet, and C. Weisbuch, *Ray Tracing for Light Extraction Efficiency (LEE) Modeling in Nitride LEDs*, in *Topics in Applied Physics*, Vol. 133 (Springer Verlag, 2013), pp. 301–340.

[35] L. Y. Kuritzky, C. Weisbuch, and J. S. Speck, *Prospects for 100% Wall-Plug Efficient III-Nitride LEDs*, Opt Express **26**, 16600 (2018).

[36] D. J. Myers, A. C. Espenlaub, K. Gelzinyte, E. C. Young, L. Martinelli, J. Peretti, C. Weisbuch, and J. S. Speck, *Evidence for Trap-Assisted Auger Recombination in MBE Grown InGaN Quantum Wells by Electron Emission Spectroscopy*, Appl Phys Lett **116**, 91102 (2020).

[37] A. C. Espenlaub, D. J. Myers, E. C. Young, S. Marcinkevičius, C. Weisbuch, and J. S. Speck, *Evidence of Trap-Assisted Auger Recombination in Low Radiative Efficiency MBE-Grown III-Nitride LEDs*, J Appl Phys **126**, 184502 (2019).

[38] Y. C. Chow, C. Lynsky, S. Nakamura, S. P. Denbaars, C. Weisbuch, and J. S. Speck, *Impact of Doped Barriers on the Recombination Coefficients of c -Plane InGaN/GaN Single Quantum Well Light-Emitting Diodes*, Appl Phys Lett **121**, 181102 (2022).

[39] C. Lynsky, G. Lheureux, B. Bonef, K. S. Qwah, R. C. White, S. P. Denbaars, S. Nakamura, Y. R. Wu, C. Weisbuch, and J. S. Speck, *Improved Vertical Carrier Transport for Green III-Nitride LEDs Using (In,Ga) N Alloy Quantum Barriers*, Phys Rev Appl **17**, 054048 (2022).

[40] Z. Quan, L. Wang, C. Zheng, J. Liu, and F. Jiang, *Roles of V-Shaped Pits on the Improvement of Quantum Efficiency in InGaN/GaN Multiple Quantum Well Light-Emitting Diodes*, J Appl Phys **116**, 183107 (2014).

[41] X. Wu, J. Liu, and F. Jiang, *Hole Injection from the Sidewall of V-Shaped Pits into c -Plane Multiple Quantum Wells in InGaN Light Emitting Diodes*, J Appl Phys **118**, 164504 (2015).

[42] W. Qi, J. Zhang, C. Mo, X. Wang, X. Wu, Z. Quan, G. Wang, S. Pan, F. Fang, J. Liu, and F. Jiang, *Effects of Thickness Ratio of InGaN to GaN in Superlattice Strain Relief Layer on the Optoelectrical Properties of InGaN-Based Green LEDs Grown on Si Substrates*, J Appl Phys **122**, 84504 (2017).

[43] Z. J. Quan, J. L. Liu, F. Fang, and F. Y. Jiang, *Effect of V-Shaped Pit Area Ratio on Quantum Efficiency of Blue InGaN/GaN Multiple-Quantum Well Light-Emitting Diodes*, Opt Quantum Electron **48**, 195 (2016).

[44] Q. Lv, J. Liu, C. Mo, J. Zhang, X. Wu, Q. Wu, and F. Jiang, *Realization of Highly Efficient InGaN Green LEDs with Sandwich-like Multiple Quantum Well Structure: Role of Enhanced Interwell Carrier Transport*, ACS Photonics **6**, 130 (2019).

[45] L. W. James and J. L. Moll, *Transport Properties of GaAs Obtained from Photoemission Measurements*, Physical Review **183**, 740 (1969).

[46] J. Peretti, H. J. Drouhin, and D. Paget, *Novel Photoemission Approach to Hot-Electron Transport in Semiconductors*, Phys Rev Lett **64**, 1682 (1990).

[47] M. Piccardo, L. Martinelli, J. Iveland, N. Young, S. P. Denbaars, S. Nakamura, J. S. Speck, C. Weisbuch, and J. Peretti, *Determination of the First Satellite Valley Energy in the Conduction Band of Wurtzite GaN by Near-Band-Gap Photoemission Spectroscopy*, Phys Rev B **89**, 235124 (2014).

[48] W. E. Spicer, *Negative Affinity 3-5 Photocathodes: Their Physics and Technology*, Applied Physics **12**, 115 (1977).

[49] S. Marcinkevičius, T. K. UŽdavinys, H. M. Foronda, D. A. Cohen, C. Weisbuch, and J. S. Speck, *Intervalley Energy of GaN Conduction Band Measured by Femtosecond Pump-Probe Spectroscopy*, Phys Rev B **94**, 235205 (2016).

[50] D. J. Myers, K. Gelžinyte, W. Y. Ho, J. Iveland, L. Martinelli, J. Peretti, C. Weisbuch, and J. S. Speck, *Identification of Low-Energy Peaks in Electron Emission Spectroscopy of InGaN/GaN Light-Emitting Diodes*, J Appl Phys **124**, 55703 (2018).

[51] D. J. Myers, K. GelŽinytė, A. I. Alhassan, L. Martinelli, J. Peretti, S. Nakamura, C. Weisbuch, and J. S. Speck, *Direct Measurement of Hot-Carrier Generation in a Semiconductor Barrier Heterostructure: Identification of the Dominant Mechanism for Thermal Droop*, Phys Rev B **100**, 125303 (2019).

[52] W. Y. Ho, A. I. Alhassan, C. Lynsky, Y. C. Chow, D. J. Myers, S. P. Denbaars, S. Nakamura, J. Peretti, C. Weisbuch, and J. S. Speck, *Detection of Hot Electrons Originating from an Upper Valley at ∼1.7 EV above the Γ Valley in Wurtzite GaN Using Electron Emission Spectroscopy*, Phys Rev B **107**, 035303 (2023).

[53] W. Y. Ho, Y. C. Chow, S. Nakamura, J. Peretti, C. Weisbuch, and J. S. Speck, *Measurement of Minority Carrier Diffusion Length in p -GaN Using Electron Emission Spectroscopy (EES)*, Appl Phys Lett **122**, 212103 (2023).

[54] D. J. Myers, Electron Emission Spectroscopy of III-Nitride Semiconductor Devices, Thesis, University of California, Santa Barbara, 2019.

[55] N. Barrett, D. M. Gottlob, C. Mathieu, C. Lubin, J. Passicousset, O. Renault, and E. Martinez, *Operando X-Ray Photoelectron Emission Microscopy for Studying Forward and Reverse Biased Silicon p-n Junctions*, Review of Scientific Instruments **87**, 53703 (2016).

[56] W. B. Joyce and S. H. Wemple, *Steady-State Junction-Current Distributions in Thin Resistive Films on Semiconductor Junctions (Solutions of ∇_2^v = ±e^v)*, J Appl Phys **41**, 3818 (1970).

[57] *Elmitec - LEEM*, https://elmitec.de/Leem.php?Bereich=LEEM3.

[58] *TVIPS - TemCam F-Series*, https://www.tvips.com/camera-systems/temcam-f-series/.

[59] S. W. King, J. P. Barnak, M. D. Bremser, K. M. Tracy, C. Ronning, R. F. Davis, and R. J. Nemanich, *Cleaning of AlN and GaN Surfaces*, J Appl Phys **84**, 5248 (1998).

[60] O. E. Tereshchenko, G. É. Shaĭbler, A. S. Yaroshevich, S. V. Shevelev, A. S. Terekhov, V. V. Lundin, E. E. Zavarin, and A. I. Besyul'kin, *Low-Temperature Method of Cleaning p-GaN(0001) Surfaces for Photoemitters with Effective Negative Electron Affinity*, Physics of the Solid State **46**, 1949 (2004).

[61] M. Sauty, C. W. Johnson, W. Y. Ho, T. Tak, Y. C. Chow, J. S. Speck, A. K. Schmid, C. Weisbuch, and J. Peretti, *Study of Cesium Deposition on GaN Photocathodes by Low Energy Electron Microscopy*, In Preparation (n.d.).

[62] *Gatan - MonoCL4*, https://www.gatan.com/techniques/cathodoluminescence.

[63] *Thermo Fisher Scientific - Apreo 2*, https://www.thermofisher.com/us/en/home/electron-microscopy/products/scanning-electron-microscopes/apreo-sem.html.

[64] *Talos™ F200X G2 TEM*, https://www.thermofisher.com/order/catalog/product/TALOSF2OOX.

[65] *Focused Ion Beam Microscopy | Microscopy and Microanalysis Facility*, https://mmf.engineering.ucsb.edu/instruments/focused-ion-beam-microscopy#fei-helios.

[66] *IMS 7f-Auto: Fully Automated High Throughput SIMS for Materials & Semiconductors l CAMECA*, https://www.cameca.com/products/sims/ims7f-auto.

[67] *MFP-3D AFM*, https://afm.oxinst.com/products/mfp-3d-afm-systems/mfp-3d-origin-afm.

[68] N. Cao, *Plasma-Etching of GaN Using (Cl 2 , BCl 3) Based Chemistry and Unaxis ICP Tool*, https://wiki.nanofab.ucsb.edu/w/images/c/cb/08-Plasma_Etching_of_GaN-RIE5.pdf.

[69] W. Y. Ho, Y. C. Chow, Z. Biegler, K. S. Qwah, T. Tak, A. Wissel-Garcia, I. Liu, F. Wu, S. Nakamura, and J. S. Speck, *Atomic Layer Etching (ALE) of III-Nitrides*, Appl Phys Lett **123**, 62102 (2023).

[70] M. Shahmohammadi, W. Liu, G. Rossbach, L. Lahourcade, A. Dussaigne, C. Bougerol, R. Butté, N. Grandjean, B. Deveaud, and G. Jacopin, *Enhancement of Auger Recombination Induced by Carrier Localization in InGaN/GaN Quantum Wells*, Phys Rev B **95**, 125314 (2017).

[71] R. Vaxenburg, A. Rodina, E. Lifshitz, and A. L. Efros, *The Role of Polarization Fields in Auger-Induced Efficiency Droop in Nitride-Based Light-Emitting Diodes*, Appl Phys Lett **103**, 221111 (2013).

[72] R. Aleksiejunas, M. Sudzius, V. Gudelis, T. Malinauskas, K. Jarasiunas, Q. Fareed, R. Gaska, M. S. Shur, J. Zhang, J. Yang, E. Kuokstis, and M. A. Khan, *Carrier Transport and Recombination in InGaN/GaN Heterostructures, Studied by Optical Four-Wave Mixing Technique*, Physica Status Solidi (C) **0**, 2686 (2003).

[73] R. Aleksiejūnas, K. Nomeika, O. Kravcov, S. Nargelas, L. Kuritzky, C. Lynsky, S. Nakamura, C. Weisbuch, and J. S. Speck, *Impact of Alloy-Disorder-Induced Localization on Hole Diffusion in Highly Excited c -Plane and m -Plane (In, Ga) N Quantum Wells*, Phys Rev Appl **14**, 054043 (2020).